

OPEN ACCESS

EDITED BY

Alessandro Stocchino, Hong Kong Polytechnic University, Hong Kong SAR, China

REVIEWED BY
Zhongya Cai,
University of Macau, China
Keshav Raja,
Florida State University, United States

*CORRESPONDENCE
Chuanyu Liu
Chuanyu.liu@qdio.ac.cn

RECEIVED 21 April 2025 ACCEPTED 06 October 2025 PUBLISHED 07 November 2025

CITATION

Lu L, Liu C, Huang RX and Wang F (2025) An energy-constrained profile parameterization of shear-driven turbulence in the interior ocean. *Front. Mar. Sci.* 12:1615741. doi: 10.3389/fmars.2025.1615741

COPYRIGHT

© 2025 Lu, Liu, Huang and Wang. This is an open-access article distributed under the terms of the Creative Commons Attribution License (CC BY). The use, distribution or reproduction in other forums is permitted, provided the original author(s) and the copyright owner(s) are credited and that the original publication in this journal is cited, in accordance with accepted academic practice. No use, distribution or reproduction is permitted which does not comply with these terms.

An energy-constrained profile parameterization of shear-driven turbulence in the interior ocean

Lei Lu^{1,2}, Chuanyu Liu^{1,2,3}*, Rui Xin Huang⁴ and Fan Wang^{1,2,3}

¹Key Laboratory of Ocean Observation and Forecasting, and Key Laboratory of Ocean Circulation and Waves, Institute of Oceanology, Chinese Academy of Sciences, Qingdao, China, ²University of Chinese Academy of Sciences, Beijing, China, ³Laoshan Laboratory, Qingdao, China, ⁴Department of Physical Oceanography, Woods Hole Oceanographic Institution, Woods Hole, MA, United States

This paper proposes an energy-constrained profile parameterization of both turbulent kinetic energy dissipation rate (ε) and vertical diffusivity (κ) , for shear instability-induced turbulence that is initiated in an initial unstable layer (IUL) where the gradient Richardson number $Ri \in (0, 0.25)$. Large-eddy simulation (LES) experiments provide the data of turbulent processes originating from Kelvin-Helmholtz instability of varied initial shear conditions. The energyconstrained framework posits ε and κ as proportional to K_a and τ^{-1} , where $K_{\rm a}$ represents available kinetic energy, measuring the released kinetic energy, au denotes turbulence evolution timescale. Both are determinable by the thickness of IUL (h_0) , buoyancy frequency (N_0) , vertical shear (S_0) , and Richardson number (Ri_0) of the IUL. Notably, unlike conventional schemes that parameterize turbulent mixing for single model grid point layer by layer, the present scheme parameterizes the turbulent mixing not only for the grid point(s) of IUL, but also for all the model grid points that are within a determined vertical turbulent penetration layer, by providing a profile of diffusivity. Therefore, the scheme is termed the energy-constrained profile parameterization (EPP). EPP aligns well with the LES results and direct microstructure measurements, outperforming existing parameterizations.

KEYWORDS

turbulent mixing, large-eddy simulation, shear instability, energy constraint, parameterization

1 Introduction

Beneath the ocean surface mixed layer (ML), shear-generated turbulence is a critical mechanism driving mixing and vertical transport in stably stratified environmental flows (Geyer et al., 2010; Smyth and Moum, 2012). Its accurate representation is vital for understanding flow dynamics and improving predictive models. A common approach to parameterizing this turbulence involves relating it to the local gradient Richardson number, $Ri = N^2/S^2$, where $N^2 = -(g/\rho)(\partial \rho/\partial z)$ is the squared buoyancy frequency, and $S^2 = (\partial u/\partial z)^2 + (\partial v/\partial z)^2$ represents the squared vertical shear.

When $Ri \leq Ri_c \approx 0.25$, shear instability becomes more likely to develop, as the destabilizing effects of vertical shear overpower the stabilizing influence of buoyancy (Howard, 1961; Miles, 1961). This critical value Ri_c marks a regime where turbulence and mixing intensify significantly. Most existing parameterization schemes for vertical mixing, such as the schemes by Pacanowski and Philander (1981) (PP81) and Peters et al. (1988) (P88), as well as the widely used K-profile parameterization (KPP) by Large et al. (1994), established a relationship between Ri and shear-driven turbulence intensity, demonstrating a sharp increase in turbulent diffusivity (κ) as Ri decreases. However, based purely on dimensional grounds, the turbulence properties need to scale not only with the Ri, but also with the forcing that drives the turbulence (Chang et al., 2005; Zaron and Moum, 2009).

Essentially, in the unforced stratified shear flows, turbulent kinetic energy (TKE) is extracted from the mean flow kinetic energy (MKE) by shear production, which is converted irreversibly into potential and internal energies by buoyancy production and turbulent dissipation, respectively (Winters et al., 1995; Smyth and Winters, 2003; Smyth et al., 2007). It means that the original energy property could be a crucial factor for the turbulent mixing parameterization.

Considering that the TKE dissipation rate ε is proportional to the ratio of TKE to the turbulent timescale τ (Moum, 1996b), Kunze et al. (1990) proposed a "reduced shear parameterization" (RSP) and parameterized turbulence dissipation rate ε as $K_{\rm a}\sigma/(\gamma+1)$ for unstable layers where $Ri \in (0, 0.25)$. Here, $K_{\rm a}$ is termed as available kinetic energy (AKE) which represents the minimum amount of kinetic energy necessary to stabilize the flow, σ represents the maximum growth rate of Kelvin–Helmholtz (KH) billows (Hazel, 1972), and γ is the mixing efficiency (Osborn, 1980). Polzin (1996) found that the RSP matched his observations well, but pointed out that there is no particular reason to use this linear instability timescale as the timescale of turbulence in this scheme. This scheme, to our knowledge, has not been applied in numerical models yet.

In addition, based on RSP, Kunze (2014) demonstrated that the Ozmidov and overturn lengthscales are larger than the thickness of the unstable layer where Ri < 0.03, so turbulence can entrain water from outside the unstable layer. Many observations and numerical studies revealed the widespread occurrence of such vertical entrainment processes in various stratified flow scenarios (e.g., Smyth et al., 2005; Inoue et al., 2012; Pham and Sarkar, 2022). These insights highlight the necessity of incorporating vertical turbulence entrainment and penetration into future parameterizations to more accurately capture the dynamics of stratified turbulence.

Constructing a new parameterization scheme is always challenging. This is because the inherent complexity of turbulence processes makes it difficult to generalize their behavior. Many previous parameterizations are largely derived from limited observational datasets, which may not have fully captured the complex and nonlinear properties of turbulence in real oceanic conditions, particularly their energetics and timescales.

In this context, large-eddy simulation (LES) is a powerful tool to analyze turbulent mixing and energy transfer processes. LES resolves turbulence at high resolution, capturing the intricate cascade of energy across scales and providing detailed insights into the evolution of turbulence, and can be easily performed under varying stratification and shear conditions. Using LES, Pham et al. (2024) parameterized the daily averaged turbulent heat flux for deep-cycle turbulence in the upper Pacific equatorial ocean, taking into account the effects of surface forcing and background flow conditions.

In contrast, this study will focus on shear-driven turbulence without surface forcing. By integrating LES simulations with the energy-constrained framework like RSP, this study aims to examine the energetics and timescale characteristics of shear-driven turbulence, and finally develop a new parameterization of it, particularly for the dynamical regime of shear instability: $Ri \in (0, 0.25)$. The proposed parameterization will be tested against observational datasets and compared with previous parameterizations. The new scheme will provide a more accurate representation of turbulent diffusivity, enhancing our understanding and modeling of turbulence in stratified shear flows.

The remainder of the paper is arranged as follows. The LES model description, parameterization framework and the observations that are used to test the new parameterization are provided in section 2. The detailed experimental results and the construction of the new parameterization are described in section 3. The test of parameterization is described in section 4. A summary and discussion are given in section 5.

2 Model setup, parameterization framework and observations

2.1 LES and experiments

The LES used in this study was originally developed by Moeng (1984) and modified by P. Sullivan (e.g., Sullivan et al., 1996). The model had been applied to the equatorial ocean by Wang et al. (1996); Wang et al. (1998) and Wang and Müller (2002). The model employs a Fourier pseudospectral method in both horizontal directions and a second-order finite difference scheme in the vertical direction. The radiation conditions are applied to the bottom boundary, allowing downward propagating internal waves to leave the system (Klemp and Durran, 1983). Periodic boundary conditions are used in the horizontal directions.

The governing equations (Equations 1.1-1.4) are

$$\frac{\partial \mathbf{u}}{\partial t} + \mathbf{u} \cdot \nabla \mathbf{u} = - \nabla p - \alpha g T + \nabla \cdot \boldsymbol{\tau}, \tag{1.1}$$

$$\nabla \cdot \mathbf{u} = 0, \tag{1.2}$$

$$\frac{\partial T}{\partial t} + \mathbf{u} \cdot \nabla T = \nabla \cdot \mathbf{q}, \tag{1.3}$$

$$\frac{\partial e}{\partial t} + \mathbf{u} \cdot \nabla e = \boldsymbol{\tau} \cdot \nabla \mathbf{u} - \alpha g q_3 - \varepsilon + \nabla \cdot 2\mathbf{K} \cdot \nabla e, \quad (1.4)$$

where $\mathbf{u} = (u, v, w)$ is the velocity, p is the pressure (normalized by a reference density), $\alpha = 2.6 \times 10^{-4} \text{ K}^{-1}$ is the thermal expansion coefficient, g is the gravitational acceleration vector, $\boldsymbol{\tau}$ is the subgrid stress tensor, T is the potential temperature, $\mathbf{q} = (q_1, q_2, q_3)$ is the subgrid heat flux, e is the subgrid-scale turbulent kinetic energy, ε is the turbulent kinetic energy dissipation rate, and \mathbf{K} is a diffusion tensor. Detailed descriptions of discretization and subgrid-scale parameterization can be found in Sullivan et al. (1996) and Wang et al. (1996). Both vertical and horizontal components of the earth's rotation are ignored.

The computational domain is 512 m \times 512 m in the horizontal directions and 256 m in the vertical direction, respectively. The domain is discretized at $\Delta x = \Delta y = \Delta z = 1$ m. Such domain sizes and grid resolutions can resolve both the "long" scale (wavelength much larger than the size of turbulent eddies) oscillations/internal waves that are observed during field measurements (e.g., Moum et al., 1992) and the small overturning scales during the evolution of shear instabilities.

To investigate the relationship between turbulence strength and background variables, we designed 27 experiments with different initial conditions of velocity and temperature, resulting in different combinations of stratification, shear, and *Ri*.

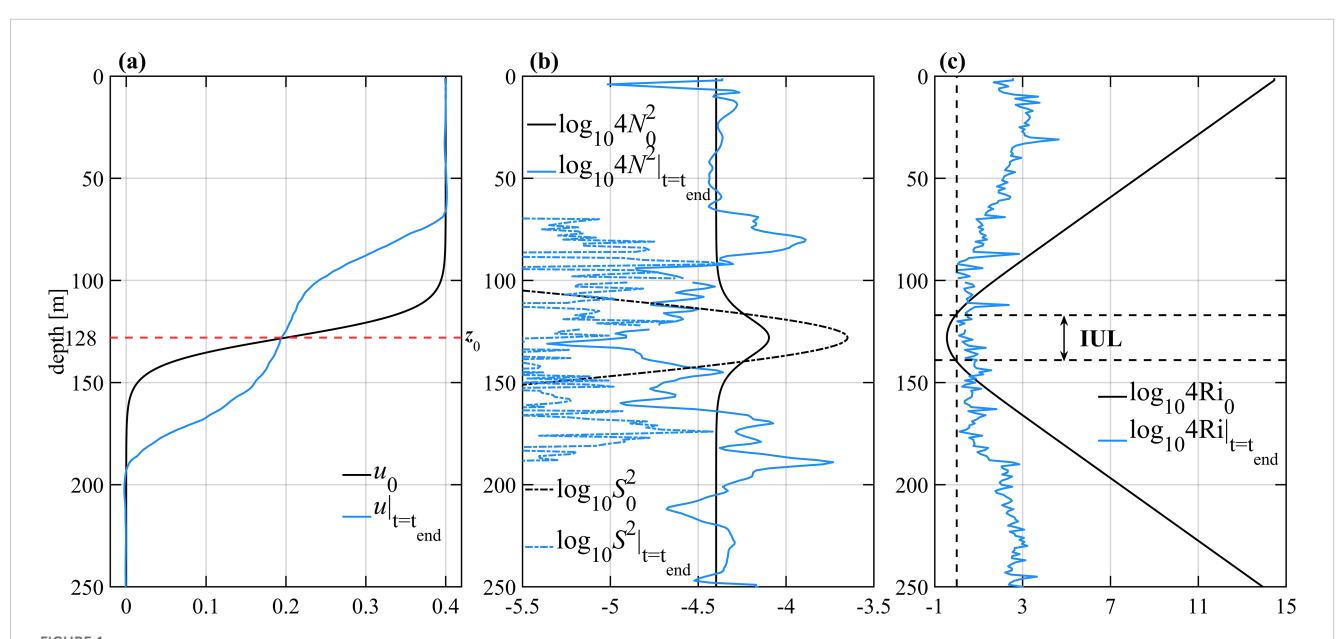
In order to assess the properties of turbulent mixing induced by a sheared and density-stratified parallel flow, initial depth-dependent profiles for the horizontal velocity u_0 and temperature T_0 , and related N_0^2 , S_0^2 and Ri_0 are fixed to the idealized and dimensional profiles (Figure 1). The explicit expressions for u_0 and squared buoyancy frequency N_0^2 are given by

$$u_0(z) = A_i \times \left[0.2 \tanh\left(\frac{z + 128}{40/3}\right) + 0.2\right] \quad (m \text{ s}^{-1}), \quad (2)$$

$$N_0^2(z) = B_i \times 0.1 \times 10^{-4} (\operatorname{sech}^2(\frac{z+128}{40/3}) + 1) \quad (s^{-2}).$$
 (3)

This flow structure follows that of Smyth and Peltier (1989). Here, corresponding A_i and B_i are the factors of u_0 and N_0^2 , respectively. u_0 decreases with depth slowly above 100 m with weak shear, and decreases with depth dramatically to nearly zero at about 150 m, resulting in large shear in-between with a squared shear peak of $2.24 \times$ 10^{-4} s^{-2} at 128 m. N_0^2 has a maximum of $0.2 \times 10^{-4} \text{ s}^{-2}$ also at 128 m; T_0 is obtained by integration of N_0^2 using a T-dependent ocean state equation. Consequently, the minimum of Rio, Rimin, reaches 0.2 at 128 m. Hereafter, the depth of 128 m is denoted as z_0 . Away from this stratified shear layer, Ri_0 is very large: it increases from its minimum to larger than 2 above 100 m and below 150 m depths. Here, the layer with Ri_0 < 0.25 is defined as the initial unstable layer (hereafter IUL). Consequently, the flow within the IUL is unstable to KH instability, which ensures the generation of turbulence after small amplitude perturbations kickstart the instability (Smyth and Peltier, 1989; Smyth et al., 2005). We note that, though these profiles cannot fully capture all potential profiles of the unstable shear layers in the ocean, they represent a large part of the characteristics of shear-driven turbulence in the stratified ocean.

A total of 27 unstable flows, with different Ri_{\min} and IULs, have been designed to obtain sufficient turbulence properties. The parameters of the flows are listed in Table 1, where the aforementioned u_0 and N_0^2 profiles are for the experiment A_7B_7 . Here we choose two other examples to depict our setting. For



Initial profile and the profile at the end of the turbulent stage ($t=t_{end}$) of experiment A_7B_7 (see text). (a) Initial zonal velocity, u_0 (solid black line), and zonal velocity at the end of the turbulent stage, $u|_{t=t_{end}}$ (solid blue line) as a function of depth; the horizontal dashed red line denotes $z_0 = 128$ m. (b) The logarithmic form of four times the squared buoyancy frequency, $\log_{10}4N_0^2$ (black solid line) and $\log_{10}4N_0^2$ (blue solid line), squared shear, $\log_{10}S_0^2$ (black dot-dashed line) and $\log_{10}S_0^2$ (blue dot-dashed line). (c) The logarithmic form of four times the Richardson number, $\log_{10}4Ri_0$ (black line) and $\log_{10}4Ri_{t=t_{end}}$ (blue line); the vertical dashed line denotes $Ri_0 = 0.25$, while the horizontal dashed black lines denote the upper and lower boundaries of the initial unstable layer (IUL).

TABLE 1 LES experiment names, denoted as A_iB_j . Here, corresponding A_i (the first line) and B_j (the first row) are the factors of u_0 and N_0^2 expressions (Equations 2, 3), respectively.

A_i B_j	0.16	0.25	0.36	0.49	0.64	0.81	1.00
1.0					A ₇ B ₅ (0.0036) (0.0571)	A ₇ B ₆ (0.0040) (0.0723)	A ₇ B ₇ (0.0045) (0.0892)
0.9					A ₆ B ₅ (0.0036) (0.0705)	A ₆ B ₆ (0.0040) (0.0892)	A ₆ B ₇ (0.0045) (0.1102)
0.8				A ₅ B ₄ (0.0031) (0.0683)	A ₅ B ₅ (0.0036) (0.0892)	A ₅ B ₆ (0.0040) (0.1129)	A ₅ B ₇ (0.0045) (0.1394)
0.7			A ₄ B ₃ (0.0027) (0.0656)	A ₄ B ₄ (0.0031) (0.0892)	A ₄ B ₅ (0.0036) (0.1165)	A ₄ B ₆ (0.0040) (0.1475)	A ₄ B ₇ (0.0045) (0.1821)
0.6		A ₃ B ₂ (0.0022) (0.0620)	A ₃ B ₃ (0.0027) (0.0892)	A ₃ B ₄ (0.0031) (0.1214)	A ₃ B ₅ (0.0036) (0.1586)	A ₃ B ₆ (0.0040) (0.2008)	
0.5	A ₂ B ₁ (0.0018) (0.0571)	A ₂ B ₂ (0.0022) (0.0892)	A ₂ B ₃ (0.0027) (0.1285)	A ₂ B ₄ (0.0031) (0.1749)			
0.4	A ₁ B ₁ (0.0018) (0.0892)	A ₁ B ₂ (0.0022) (0.1394)	A ₁ B ₃ (0.0027) (0.2008)				

The upper and lower numbers in the bracket are the N_0 max and Ri_{\min} of the corresponding initial profiles, respectively.

example, in experiment A_6B_6 , the initial zonal velocity u_0 in A_7B_7 is multiplied by a constant factor $A_6=0.9$, which results in a S_0^2 that is 0.81 times that of experiment A_7B_7 ; at the same time, N_0^2 is multiplied by $B_6=0.81$, thus the Ri_0 profile of A_6B_6 remains the same as that of experiment A_7B_7 . In experiment A_6B_5 , the initial zonal velocity u_0 in A_7B_7 is multiplied by a constant factor $A_6=0.9$, but N_0^2 is multiplied by a constant factor $B_5=0.64$; as a result, the stratification weakens more than the shear, and the profile of Ri_0 decreases, reaching a minimum of 0.05. Based on this rule, the other 24 profiles are designed. The factors to u_0 , named u_0 , named u_0 , increase from 0.4 to 1.0, while the factors to u_0 , named u_0 ,

We note that, because our study is focused on the turbulent mixing in the interior ocean, the surface forcings, including both the wind-stress-induced friction velocity and the surface heat/buoyancy flux, are set to zero in the LES experiments. This avoids the influence of boundary forcing on turbulence just below the ML base (Zaron and Moum, 2009). In addition, large-scale forcing that represents the maintenance of the background flow via larger-scale motions (Wang et al., 1998) is not set, either. As such, each of our experiments documents a non-forced evolution of turbulence, which provides 'pure' KH instability-induced turbulence data; this contrasts with the observed turbulence which could result from

more complex processes. Due to the absence of both the external forcing and large-scale forcing, the turbulence decays rapidly which usually lasts for less than 24 hours.

2.2 Fundamental variables based on the initial conditions

Since the instability develops from the IUL, the initial variables, $\overline{N_0}$, $\overline{S_0}$ and $\overline{Ri_0}$ are vertically averaged over the IUL. The thickness of IUL (IULT, denoted as h_0) is also considered an important initial variable. They are used for subsequent calculation and parameterization.

2.3 Turbulent layer and turbulent stage in the LES

2.3.1 the turbulent layer

Since a significant portion of the computational vertical layers and simulation time involves laminar flow above and below the turbulent layer, averaging turbulent statistics over the laminar regime will result in failure to accurately represent the turbulent layer properties. Smyth et al. (2005) found that the turbulent layer roughly coincided with the initial shear layer they identified, therefore they suggested that the turbulent layer can be isolated

effectively from the laminar region by two isopycnic surfaces. Building on this idea, in this study, the upper and lower boundaries of the turbulent layer (hereafter TL) are defined by two surfaces, upon which the zonal velocities had the values of the upper and lower boundaries of the IUL at each moment (Figure 2).

2.3.2 The turbulent stage and timescale τ_{LES}

A method needs to be adopted to objectively determine the turbulent stage. As for its definition, TKE is employed as a quantitative measure, because TKE is a direct measure of turbulence intensity and is also representative of turbulence generation and dissipation (Tong et al., 2022). However, using a fixed TKE threshold cannot solve the problem of the dependence of TKE on N_0 . Here, an appropriate value of 10% of the maximum TKE over the domain and simulation time for each experiment is chosen as the threshold to identify the time range. The 2 nodes at the time axis at which the vertically averaged TKE within the TL exceeds the threshold are defined as the start and end of the turbulent stage (denoted as t_{start} and t_{end}). The turbulent duration τ_{LES} is defined naturally as the difference between these 2 nodes (Figure 2). Within the turbulent duration, the TKE is firstly increased and then dissipated. Thus au_{LES} can be used as the timescale of the TKE evolution. Subsequent statistical calculations are performed in the TL and turbulent stage. τ_{LES} is a key variable to be parameterized.

2.4 Turbulent parameters in LES

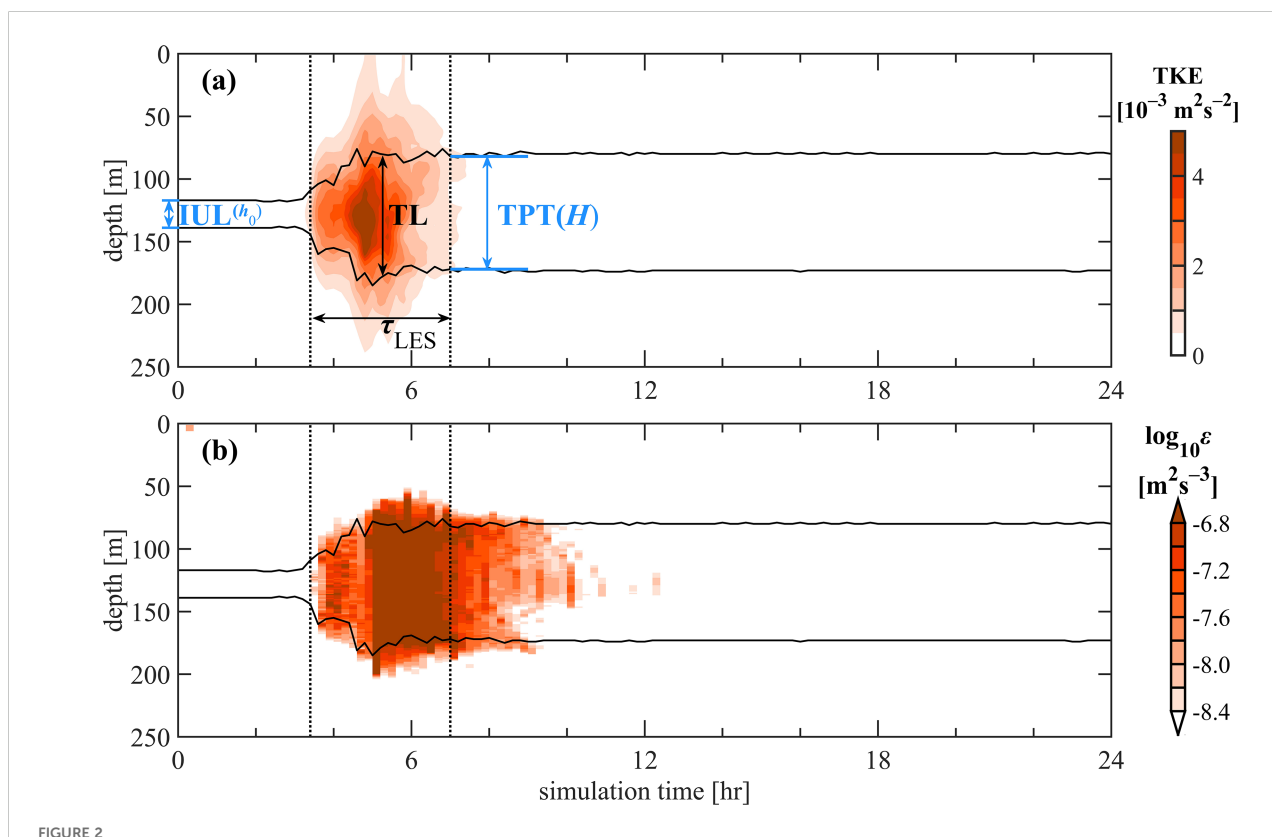
As the energy sources and sinks of turbulent evolution (Figure 3a), within the TL and over the turbulent stage, the energy transferred via shear production $E_{SP_{LES}}$, the energy transferred via turbulent dissipation $E_{\varepsilon_{LES}}$ and the energy transferred via buoyancy production $E_{B_{LES}}$ can be directly calculated from the LES outputs by the following equations:

$$E_{SP_{LES}} = \frac{1}{z_2 - z_1} \int_{z_2}^{z_2} \int_{t = t_{out}}^{t = t_{out}} -\widetilde{u'w'} \frac{\partial \tilde{u}}{\partial z} dt \quad dz$$
 (4)

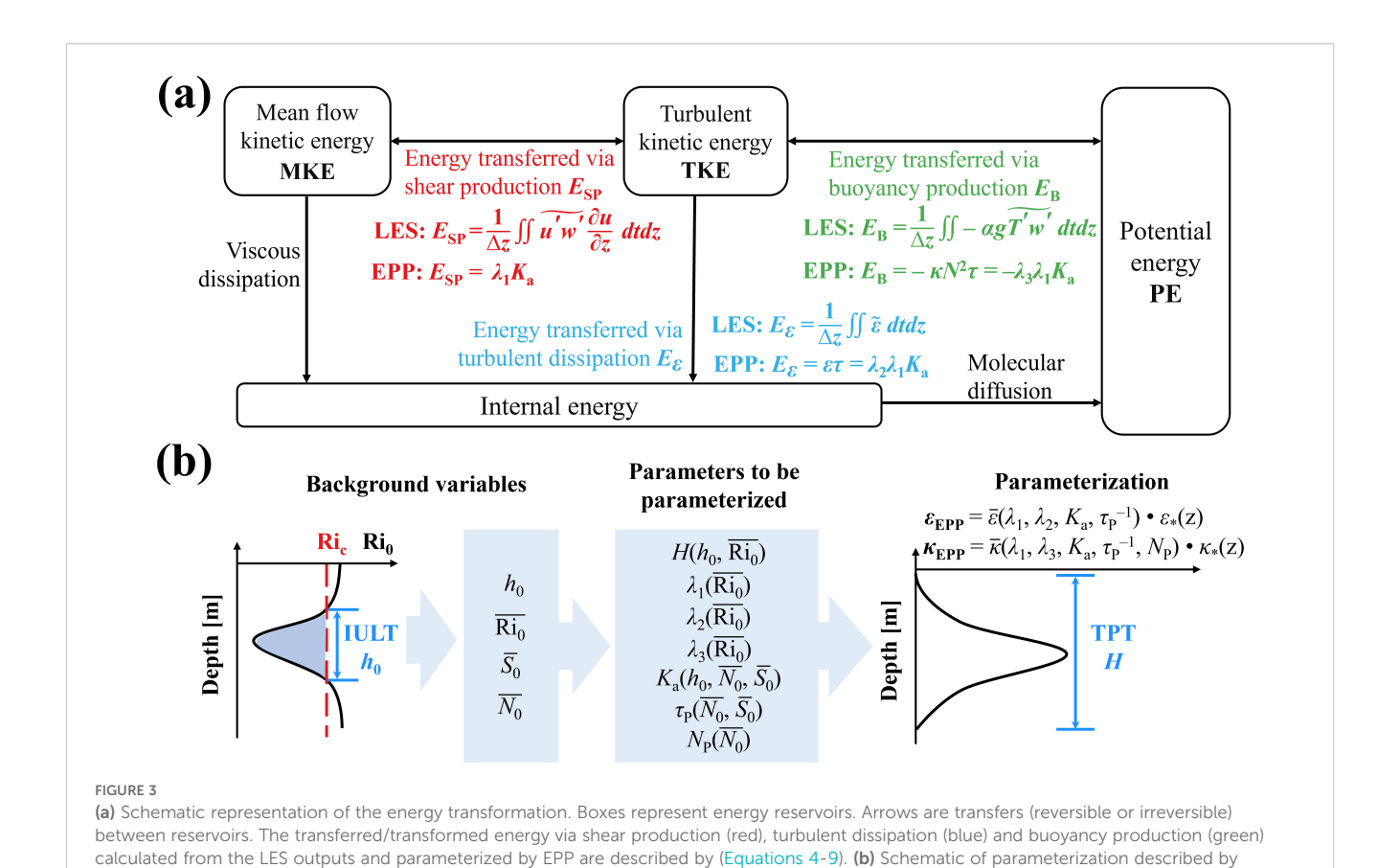
$$E_{\varepsilon_{\text{LES}}} = \frac{1}{z_2 - z_1} \int_{z_1}^{z_2} \int_{t = t_{\text{start}}}^{t = t_{\text{end}}} \tilde{\varepsilon} \quad dt \quad dz$$
 (5)

$$E_{B_{LES}} = \frac{1}{z_2 - z_1} \int_{z_1}^{z_2} \int_{t = t_{start}}^{t = t_{end}} -ag\widetilde{T'w'} dt \quad dz$$
 (6)

$$E_{SP_{LES}} + E_{B_{LES}} - E_{\varepsilon_{LES}} \approx 0,$$
 (7)



Time evolution of horizontal mean (a) TKE and (b) TKE dissipation rate ε as a function of depth for experiment A_7B_7 . The Black lines denote the boundary of the turbulent layer. Horizontal blue solid lines (left) denote the upper and lower boundary of the initial unstable layer (IUL) while the horizontal blue solid lines (right) denote the upper and lower boundary of turbulent penetration, which is defined as the thickness of turbulent penetration (TPT). The vertical black dashed lines denote the start and end of the turbulent stage and the duration τ_{LES} is defined as the difference between these 2 time nodes.



where t_{start} and t_{end} are the start and end of the turbulent stage, and z_1 and z_2 are the upper and lower boundaries of the TL. Primes and tildes represent the deviations from the horizontal mean, and the horizontal average, respectively.

(Equations 10-15)

The 3D (horizontally over the domain and vertically over the TL) and temporally (over the turbulent stage) averaged TKE dissipation rate ε_{LES} , turbulent diffusivity κ_{LES} and buoyancy frequency N_{LES} can be directly calculated from the LES outputs by

$$\kappa_{LES} = \frac{1}{z_2 - z_1} \int_{z_1}^{z_2} -\frac{\left\langle \widetilde{T'w'} \right\rangle}{\partial \left\langle \widetilde{T} \right\rangle / \partial z} dz$$

$$\varepsilon_{LES} = \frac{1}{z_2 - z_1} \int_{z_1}^{z_2} \left\langle \widetilde{\varepsilon} \right\rangle dz$$

$$N_{LES} = \frac{1}{z_2 - z_1} \int_{z_1}^{z_2} \left\langle \widetilde{N} \right\rangle dz$$

where the angle brackets represent the temporal average over the turbulent stage.

In this study, the LES-provided ε_{LES} , κ_{LES} , τ_{LES} , N_{LES} , $E_{SP_{LES}}$, $E_{\varepsilon_{LES}}$ and $E_{B_{LES}}$ will be used as the "true" values, based on which the new parameterization would be built based on the initial variables like h_0 , $\overline{N_0}$, $\overline{S_0}$ and $\overline{Ri_0}$ (Figure 3b).

2.5 Energy constraint framework

 $E_{SP_{LES}}$ comes from the release of MKE, which is approximately equal to the difference in kinetic energy between the initial unstable flow and the quiescent flow after turbulence. In Figures 1b, c, at the end of the turbulent stage, the strength of shear within the TL is reduced, and the mean Ri is close to about 0.25 at the center and boundary of the TL. This indicated that the flow now reaches a marginally stable state (Thorpe and Liu, 2009).

Based on this feature, Kunze et al. (1990) assumed that the shear in an unstable stratified shear flow would be reduced if turbulent fluxes raised the $Ri=Ri_0<0.25$ to Ri=0.25. Assuming that shear and stratification in the IUL are constant, the difference in kinetic energy between the initial unstable state and the final state of marginal instability is defined as the AKE (K_a) , and is calculated as $K_a=h_0^2(S^2-4N^2)/24$. For nonlinear shear profiles like ours, K_a can be calculated as $h_0^2 = \frac{3}{2} (10^2 - 4N_0^2)/24$, where overbar represents the vertical average over the IUL. Though this computational approach scarifies certain physical fidelity compared to the rigorous numerical integration method, their values are consistent to a large extent (not shown); therefore, for calculation efficiency, we adopt this convenient method in the present study.

However, it is noted that the AKE (K_a) is different from $E_{SP_{LES}}$. $E_{SP_{LES}}$ represents the real released MKE throughout the TL turbulent processes, which is calculated from the LES results via (Equation 4) and is shown in Figure 3a. K_a is proposed for the purpose of parameterization, which represents the idealized amount of MKE released through the instability, without considering the complex energetics. For this reason, let $E_{SP_{LES}}$ be expressed as

$$E_{SP_{IES}} = \lambda_1 K_a, \tag{8}$$

where the parameter λ_1 is introduced in detail in the following framework of parameterization construction.

Furthermore, another parameter $\lambda_2 = E_{\mathcal{E}_{LES}}/E_{SP_{LES}}$ is introduced so that. is parameterized. Similarly, a third parameter $\lambda_3 = -E_{B_{LES}}/E_{SP_{LES}}$ is introduced. Under an assumption that the input energy is either transferred to potential energy or internal energy over the whole turbulent stage, λ_3 is naturally equal to $1 - \lambda_2$ (Figure 3a). Then, the mean $E_{\mathcal{E}_{LES}}$ and $E_{B_{LES}}$ can be expressed by considering the turbulent timescale τ_{LES} as:

$$E_{\varepsilon_{LES}} = \varepsilon_{LES} \cdot \tau_{LES} = \lambda_2 \lambda_1 K_a,$$
 (9.1)

$$E_{B_{LES}} = \kappa_{LES} \cdot N_{LES}^2 \cdot \tau_{LES} = -\lambda_3 \lambda_1 K_a. \qquad (9.2)$$

Here, λ_1 , λ_2 and λ_3 are variables to be parameterized by $\overline{Ri_0}$. In sum, for each experiment, K_a is calculated by initial variables, while the energy transferred via shear production $(E_{SP_{LES}})$ is calculated from LES outputs. By equating the parameterized $E_{SP_{LES}}$ to the K_a (Equation 8), λ_1 is derived for each experiment. Through regression analysis, λ_1 is parameterized as a function of $\overline{Ri_0}$. Similarly, parameterizations for λ_2 , λ_3 , N_{LES} and τ_{LES} are obtained. Ultimately, parameterized expressions for the turbulent diffusivity and dissipation rate are derived (Figure 3b).

2.6 Observations

A dataset of observations is collected to verify our parameterization. First, turbulence activity was measured during the Tropical Instability Wave Experiment (TIWE) in the fall of 1991 at 0°, 140°W (Lien et al., 1995). During this experiment, two overlapping time series of measurements were made from two independent ships, *Wecoma* and *Moana Wave*, so the method and data can be compared and validated. 3918 casts and 2072 casts of microstructure temperature, conductivity, and shear measurements in the upper 200 m were made using the profiler CHAMELEON and the Advanced Microstructure Profiler (AMP). The horizontal velocity was measured by the ship-mounted Acoustic Doppler Current Profilers (ADCPs) with the vertical resolution of approximately 8 m.

The TKE dissipation rate ε_{obs} is estimated by the method of sensing small-scale shears from the free-falling profilers (Moum et al., 1995). κ_{obs} is calculated as $\gamma \varepsilon_{obs}/N^2$, where γ is taken as a common value of 0.2 (Lien et al., 1995; Zaron and Moum, 2009). Because of the occasional necessity of repairs and delays caused by other operational difficulties, the time series of profiles was unevenly sampled. To simplify the calculation, all data were

averaged hourly with the vertical resolution of 1 m. In the next subsections, we will further process this dataset to comply with our EPP scheme.

Researchers usually directly apply a parameterization to observed hydrologic data to evaluate its performance. However, we note that it is difficult to fairly evaluate the performance this way. Firstly, observational data often lack the precise background variables that are required to initialize the potential turbulent events, unlike the well-controlled initial conditions in LES experiments. The so-called background fields may also have undergone the influence of prior turbulence. Secondly, the observed mixing coefficients (such as ε and κ) are subject to other larger-scale forces, such as advection and shear production, which is also unlike the freely developed turbulence as seen in LES. Lastly, turbulence observed at an observational site may originate from remote locations rather than local instability.

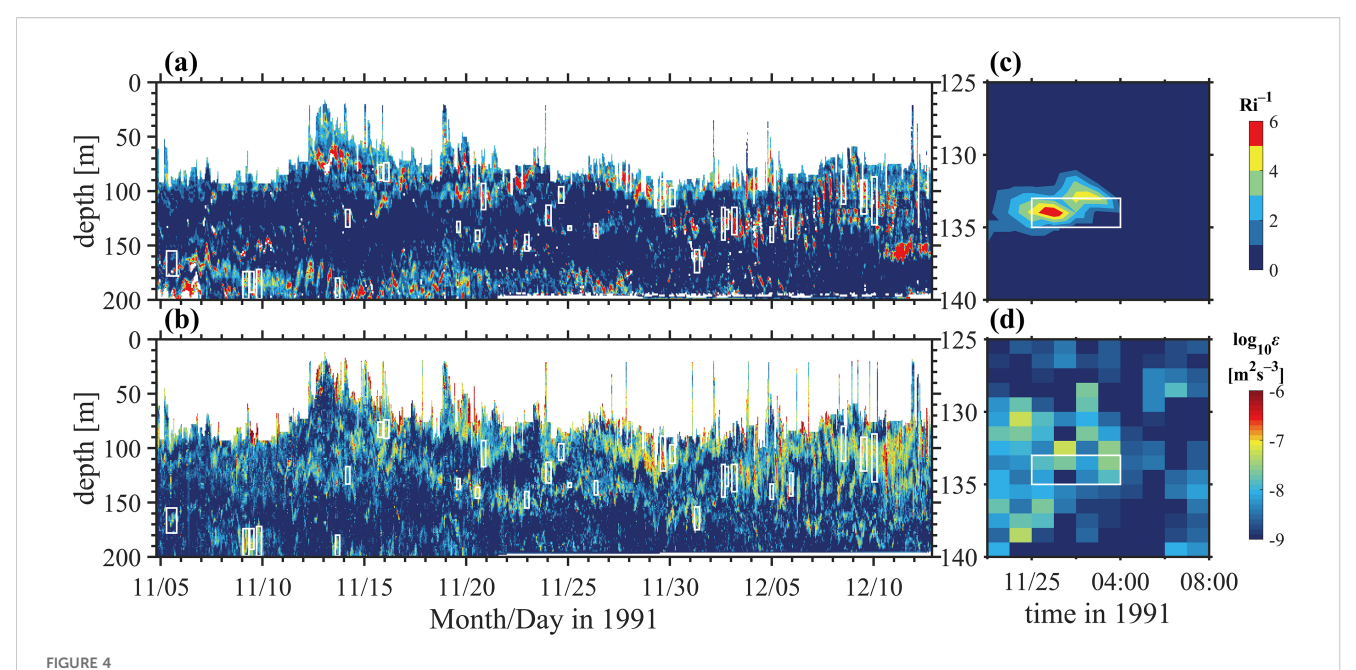
To compare EPP with observations, some turbulent events are picked out (marked by the white square in Figures 4a, b). As shown in Figures 4c, d, such turbulent events resemble LES experiments. Enhanced turbulence follows a fluid state within an IUL with $Ri \in (0, 0.25)$.

3 Turbulent properties and the parameterizations

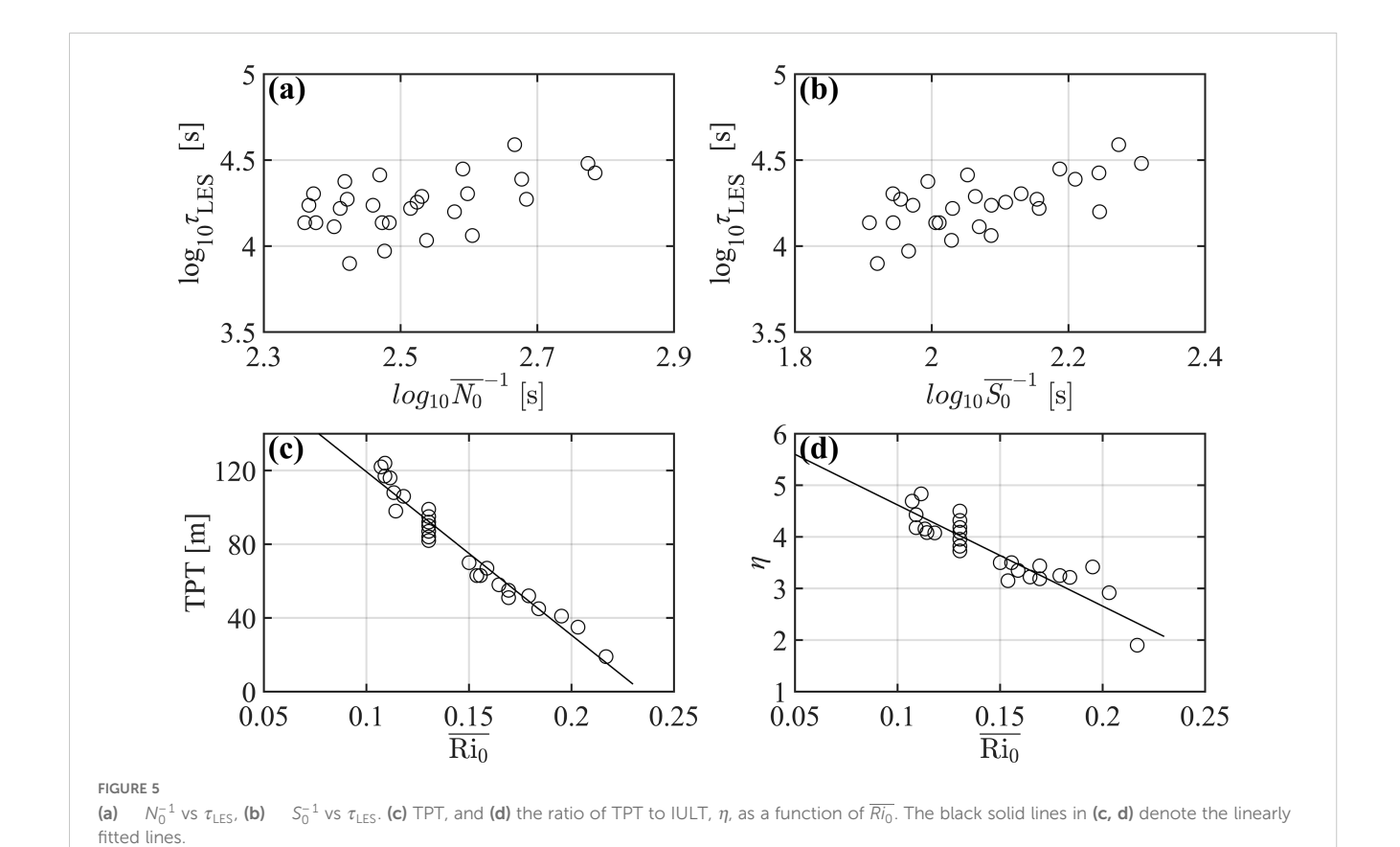
3.1 Temporal evolution of turbulent properties: TKE, ε and TL

The turbulent kinetic energy (TKE) and its dissipation rate, ε , are important metrics describing the development and decay of turbulence. The temporal variability of horizontally averaged TKE and ε over each model layer, and the identified TL and turbulent stage for experiment A_7B_7 are shown in Figure 2. τ_{LES} is about 4 hours. TKE increases rapidly in the domain of IUL during the onset of the turbulent stage. TKE surges to a peak ($\sim 5 \times 10^{-3}$ m² s $^{-2}$) within about 1 hour in the domain of IUL. Then TKE declines gradually to the background value over 3 hours. ε increases and maintains a value ranging $4 \times 10^{-9} - 4 \times 10^{-8}$ m² s $^{-3}$ during the first 2 hours of the turbulent stage. After this, ε surges to more than 1.6×10^{-7} m² s $^{-3}$ and keeps for about 2 hours. Although a short period with high ε is excluded from the turbulent stage, most of the turbulent characteristics have been captured. ε for the 27 experiments show a similar evolution as described above.

In addition, due to the vertical penetration of the turbulence, the TL becomes thicker rapidly. The thickness of the TL at the end of the turbulent stage is defined as the turbulent penetration thickness (hereafter TPT, denoted as H). H (90 m) is approximately 4 times larger than h_0 (22 m) in experiment A_7B_7 (Figure 2). Strong vertical turbulent momentum and buoyancy fluxes therein result in a decrease in the temperature and velocity above the z_0 and an increase of them below the z_0 (Figure 1a). This variation has been shown in the direct numerical simulation results of Smyth and Winters (2003) and the CROCO ocean model results of Penney et al. (2020).



Depth-time plots of (a) inverse Richardson number Ri^{-1} and (b) ε of TIWE. (c, d) as in (a, b) but for the turbulent events described in section 2.6. Times are UTC. White boxes represent the turbulent events. Values are blanked (white) in the ML and deep cycle layer in (a, b). The depth of ML is defined as the minimum depth within which the density is 0.01 kg m⁻³ heavier than the surface value while the DCL base is defined as the deepest depth below the ML at which Ri< 0.25 (Lien et al., 1995).



However, there is a significant difference in τ_{LES} across the 27 experiments, owing to the varied initial conditions (Figures 5a, b). τ_{LES} varies between 7920 s and 38880 s, and increases with increasing N_0^{-1} which is often quoted for turbulence generation and dissipation (e.g., Moum, 1996b). Although τ_{LES} (i.e., 13680 s) for experiment A_7B_7 is much longer than the timescale N_0^{-1} (i.e., 250 s), it is comparable with the value of Smyth et al. (2005). When $N_0 \approx 1 \times 10^{-2} \, \rm s^{-1}$ (their Figure 1), their duration is about 5000 s and 50 times N_0^{-1} . It can also be found that τ_{LES} appear to increase with increasing S_0^{-1} , which is consistent with the results of Watanabe and Nagata (2021).

The TPTs of 27 experiments range from 20 m to 120 m, and their variations are significantly correlated with the $\overline{Ri_0}$ (Figure 5c). A linear regression of TPT on $\overline{Ri_0}$ can explain 96% of the variance. However, the IULT is also related to $\overline{Ri_0}$, thus the ratio of TPT to IULT, η , is a good index representing the penetration intensity of turbulence. In Figure 5d, η is a monotone-decreasing function of $\overline{Ri_0}$. TPTs can reach nearly 5 times the IULTs when the $\overline{Ri_0}$ is about 0.1, which is comparable to the values of 2–3 in Smyth et al. (2005) and 5 in Penney et al. (2020). Different from the theoretical results of Kunze (2014), turbulent entrainment can also occur even for $Ri \subseteq (0.03, 0.25)$.

3.2 Parameterization of ε_{IFS}

To parameterize E_{SP} with $K_{\rm a}$, we calculated λ_1 of each experiment, and found that λ_1 varies between 1.5 and 25 (Figure 6a). When the velocity after simulated turbulent mixing is close to the prescribed idealized velocity of marginal instability, λ_1 is small and close to 1; however, the more they differ from each other, the more MKE is released and the value of λ_1 is larger than 1.

Calculation based on the LES results reveals that λ_2 varies between 0.38 and 0.69 (Figure 6b). The larger λ_2 is, the larger proportion of TKE is dissipated into the internal energy. It is noted that λ_3 is intrinsically the flux Richardson number R_f , and λ_3/λ_2 is another measure of mixing efficiency γ which is the ratio of $-E_B$ to E_{ε} (Smyth et al., 2001; Inoue and Smyth, 2009). We found that the values of γ range from about 0.4 to 1.4, which are larger than the commonly used value of 0.2; the underlying reason is that the calculation of γ includes the development stage of turbulence where γ is believed large (Smyth, 2020). Actually, γ can be larger than 1 when the flux Richardson number R_f is large, as seen in many numerical simulations and oceanic measurements (Moum, 1996a; Smyth et al., 2001; Salehipour and Peltier, 2015).

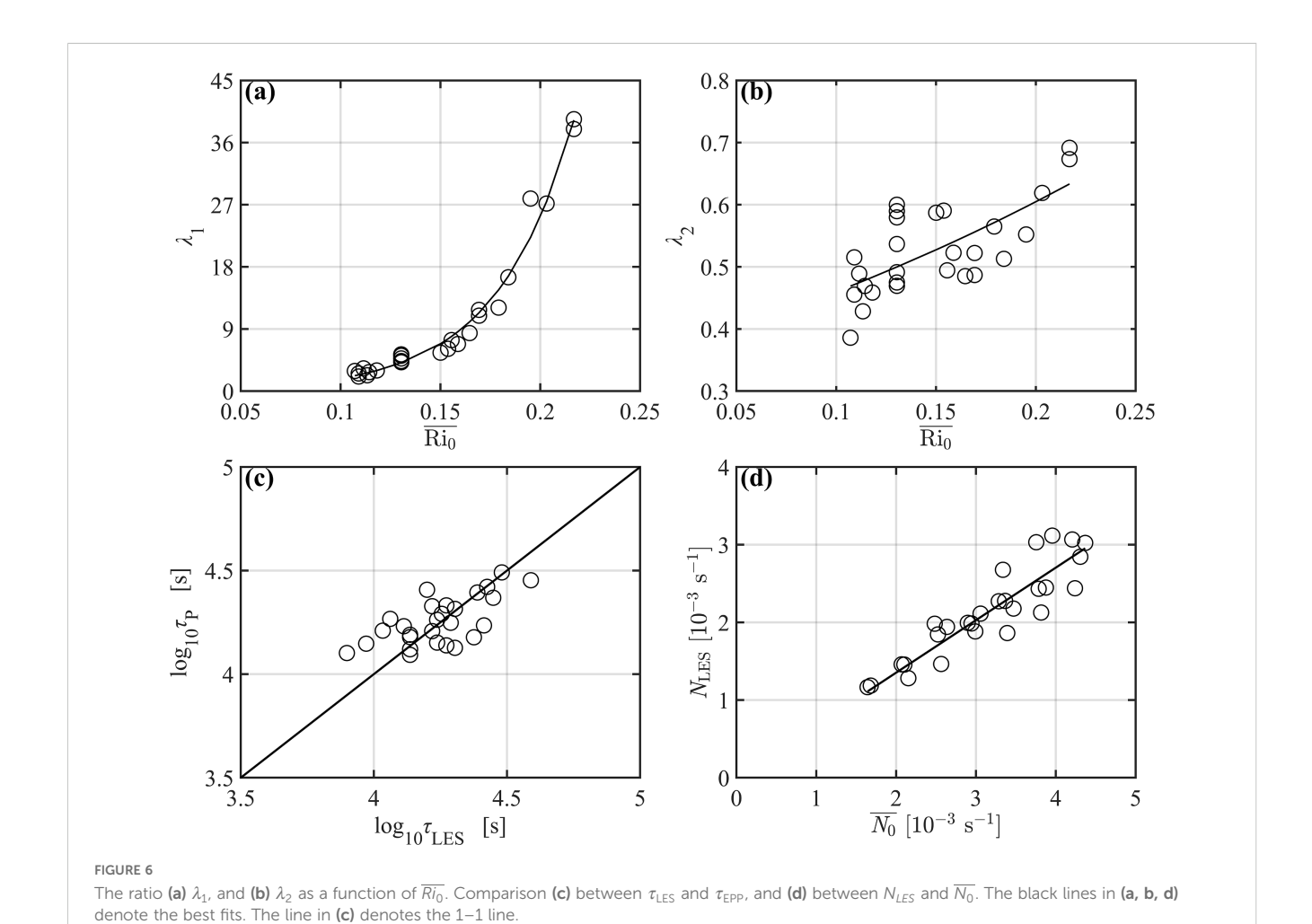


TABLE 2 Coefficient values of parameterizations.

Coefficients	а	b	С	d	f
values	0.1364 (0.0852, 0.1876)	26.11 (24.26, 27.96)	0.3497 (0.2865, 0.4130)	2.7390 (1.6000, 3.8780)	0.0404 (0.0249, 0.0560)
Coefficients	g	h		j	
values	0.0286 (0.0208, 0.0364)	0.6761 (0.6459, 0.7063)	-19.61 (-23.13, -16.08)	6.58 (6.04, 7.12)	

The numbers in the bracket are the confidence intervals.

Finally, to parameterize E_{SP} , E_{ε} and E_B with K_a , λ_1 and λ_2 should be parameterized at first. We found that λ_1 and λ_2 are good functions of $\overline{Ri_0}$ (Figures 6a, b). λ_1 and λ_2 both increase with increasing $\overline{Ri_0}$. λ_1 increases exponentially with $\overline{Ri_0}$ while λ_2 increases almost linearly with $\overline{Ri_0}$. Based on the data, we give the following fitting functions,

$$\lambda_{1_p} = ae^{b\overline{Ri_0}}, \ and \ \lambda_{2_p} = ce^{d\overline{Ri_0}}.$$
 (10)

The regressions are shown in Figures 6a, b, respectively. Coefficient values and confidence intervals are listed in Table 2, and the residuals are presented in the Supplementary Material. λ_{1p} can explain about 98% of the variance of λ_1 (R² = 0.98), while λ_{2p} can explain about 47% of the variance of λ_2 (R² = 0.47). The low R² value indicates that nonlinear processes (e.g., vortex pairing) significantly modulate λ_2 . Nevertheless, $\overline{Ri_0}$ remains an important control parameter.

In Equation 9.1, timescale τ_{LES} need to be parameterized. Previously, $\sigma = (S-2N)/4$ was used by Kunze et al. (1990) to estimate the inverse timescale for the growth of small amplitude billows based on linear stability analysis (Hazel, 1972), while N^2/S was used to estimate the inverse timescale for the dissipation stage after the inception of shear turbulence based on the laboratory data (Thorpe, 1973). Polzin (1996) indicated that durations for turbulent events of observations during the North Atlantic Tracer Release Experiment encompass both growth and dissipation timescales. Considering that τ_{LES} is the full duration of turbulent evolution, which includes both the growth and decay stages based on nonlinear numerical simulations, we parameterize the turbulent timescale τ_{LES} as a linear combination of the two mentioned timescales,

$$\tau_{P}^{-1} = f \frac{(\overline{S_0} - 2\overline{N_0})}{4} + g \frac{\overline{N_0}^2}{\overline{S_0}},$$
 (11)

where f and g are determined to be 0.04044 and 0.02861 by two-variable linear regression. The parameterization of τ_{LES} , i.e., τ_P , explains about 50% of the variance of τ_{LES} ($R^2 = 0.50$) as shown in Figure 6c. This expression is simple and easy to be used in the parameterization scheme. Accordingly, Equation 9.1 becomes:

$$\varepsilon_{EPP} = ace^{(b+d)\overline{Ri_0}} \cdot h_0^2 \frac{\overline{S_0^2 - 4N_0^2}}{24} \cdot (f \frac{(\overline{S_0} - 2\overline{N_0})}{4} + g \frac{\overline{N_0}^2}{\overline{S_0}}).$$
 (12)

Equation 12 is the energy-constrained parameterization for the TKE dissipation rate induced by the KH instability for the IUL where $Ri \in (0, 0.25)$, which is represented by the original background variables.

3.3 Parameterization of κ_{LFS}

In the meanwhile, it is found that the stratification N_{LES} in Equation 9.2 has a significant linear relationship with the initial value $\overline{N_0}$, i.e., $N_P = h\overline{N_0}$ (Figure 6d). where h is determined to be 0.6761. N_P explains about 82% of the variance of N_{LES} ($R^2 = 0.82$). In addition, λ_3 is parameterized as $1 - \lambda_{2_P}$. Accordingly, Equation 9.2 becomes:

$$\kappa_{EPP} = (1 ce^{d\overline{Ri_0}}) \cdot ae^{b\overline{Ri_0}} \cdot h_0^2 \frac{\overline{S_0^2 - 4N_0^2}}{24} \cdot (f \frac{(\overline{S_0 - 2N_0})}{4} + g \frac{\overline{N_0^2}}{\overline{S}}) \cdot (h\overline{N_0})^{-2}.$$
(13)

Equation 13 is the energy-constrained parameterization for κ of the KH instability-induced turbulence for the IUL where $Ri \in (0, 0.25)$, which is represented by the original background variables.

The last key property of the present parameterization lies in the vertical extension of the turbulent mixing. An important information obtained from both previous studies and the present LES results is that the shear instability-driven turbulence is not confined within the IUL, but extends to the neighboring layers. This phenomenon represents the release of accumulated energy from a potentially unstable fluid system. The TPT should represent the outer boundary of the system where the energy can be extracted. Thinking from this way, it is necessary to parameterize κ within the TPT, rather than at the grid points of $Ri \in (0, 0.25)$ only like in the previous parameterizations.

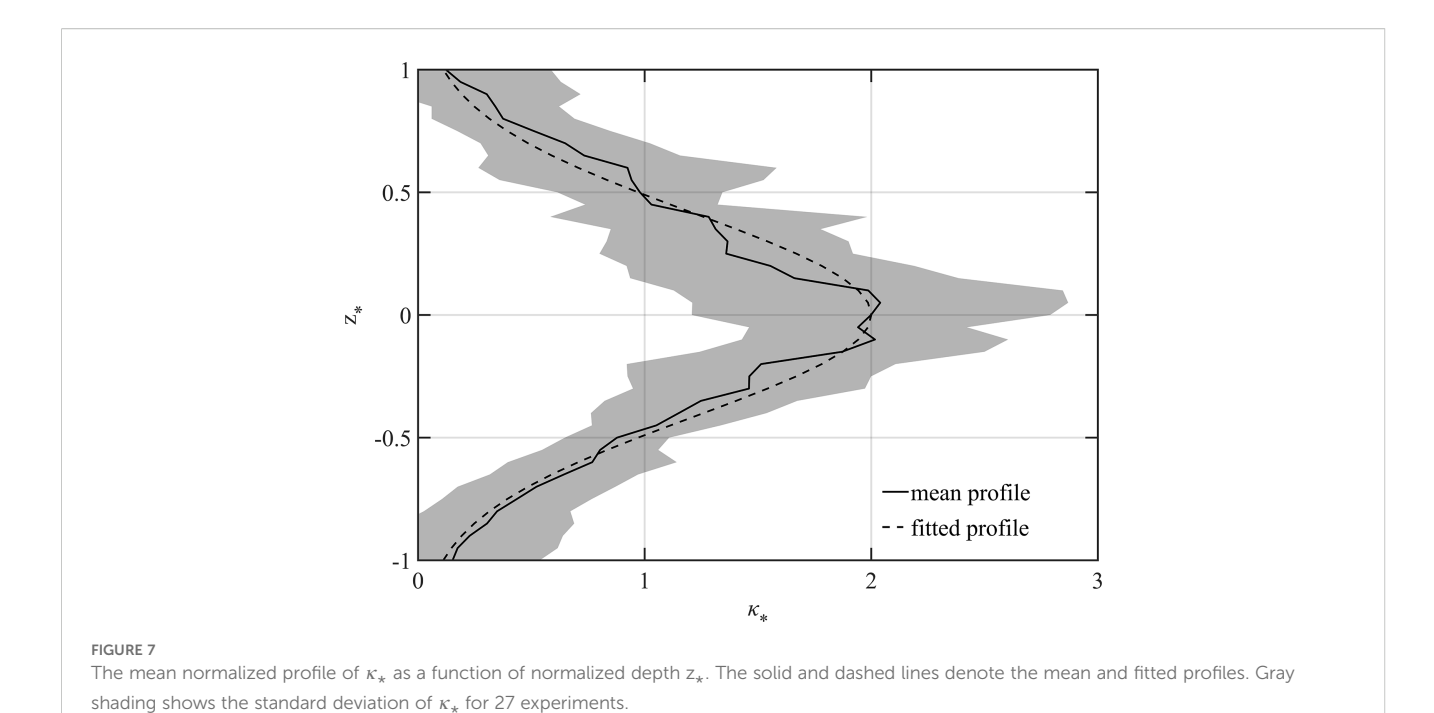
The suitable parameterization for this issue includes two steps. The first step is to identify TPT and represent it with original background variables, while the second step is to redistribute κ vertically within TPT.

Firstly, as described in section 3a, the ratio of TPT to IULT, η , varies from 2 to 5; furthermore, it can be fitted as a linear function of $\overline{Ri_0}$ (Figure 5d)

$$\eta_P = i\overline{Ri_0} + j, \tag{14}$$

where i and j are determined as –19.61 and 6.58. η_P explains about 82% of the variance of η (R² = 0.82). In practice, IULT can be determined by the grid spacing of the oceanic numerical model. Given that η can be obtained by $\overline{Ri_0}$, the TPT can also be obtained easily, providing the layers where the parameterization should be exerted.

Secondly, the vertical distribution of κ should be provided. The previous discussion and parameterization mainly focused on the mean κ_{LES} averaged vertically over the TPT under the assumption of 3D homogeneity of turbulence (Kaltenbach et al., 1994; Shih et al., 2005). Whereas, κ can be also calculated layer by layer, which can provide the



vertical pattern of κ within the TL. Specifically, for each experiment, the κ profile is calculated first, and then it is normalized by κ_{LES} to get κ_* , in the meanwhile, z is normalized by TPT to get z_* . Finally, the normalized profiles for 27 experiments are averaged, which is shown in Figure 7. It is found that κ_* reaches its maximum value which is about 2 times the vertical average at the center of TPT where Ri_0 is the minimum. Out of the deeper and shallower boundaries of TPT, κ_* rapidly decreases to almost 0. Observed diffusivity profiles resulting from KH billow breakdown in the Changjiang Estuary closely match this vertical distribution (Tu et al., 2024). This pattern of normalized profile can be described by the fitting function:

$$\kappa_{\star} = 2e^{-1.7z_{\star}^2},$$
(15)

where z_* represents the normalized depth of TPT. The fitted profile is very close to the actual mean profile. The profile of κ is obtained by multiplying κ_{EPP} in Equation 13 by κ_* . Till now, we have finished building the new parameterization for the shear instability-driven vertical mixing in the interior ocean (Equations 13, 15).

Overall, given the new parameterization is based on an energyconstrained framework and provides the vertical diffusivity profile, it is named the energy-constrained profile parameterization, and abbreviated as EPP.

4 Comparison of the EPP with LES data, observations and existing parameterizations

In this subsection, we test the proposed EPP scheme, (Equations 12-15), against the LES data and the observations, and also compare them with existing parameterizations.

4.1 Compare ε_{EPP} and κ_{EPP} with LES data

It should be noted that, although the EPP schemes are based on the same set of data as ε_{LES} and κ_{LES} , thus are non-independent, they are constructed according to the theoretical framework of energy constraint, rather than by simply fitting to ε_{LES} and κ_{LES} . Therefore, ε_{LES} and κ_{LES} of LES can be used to test our scheme.

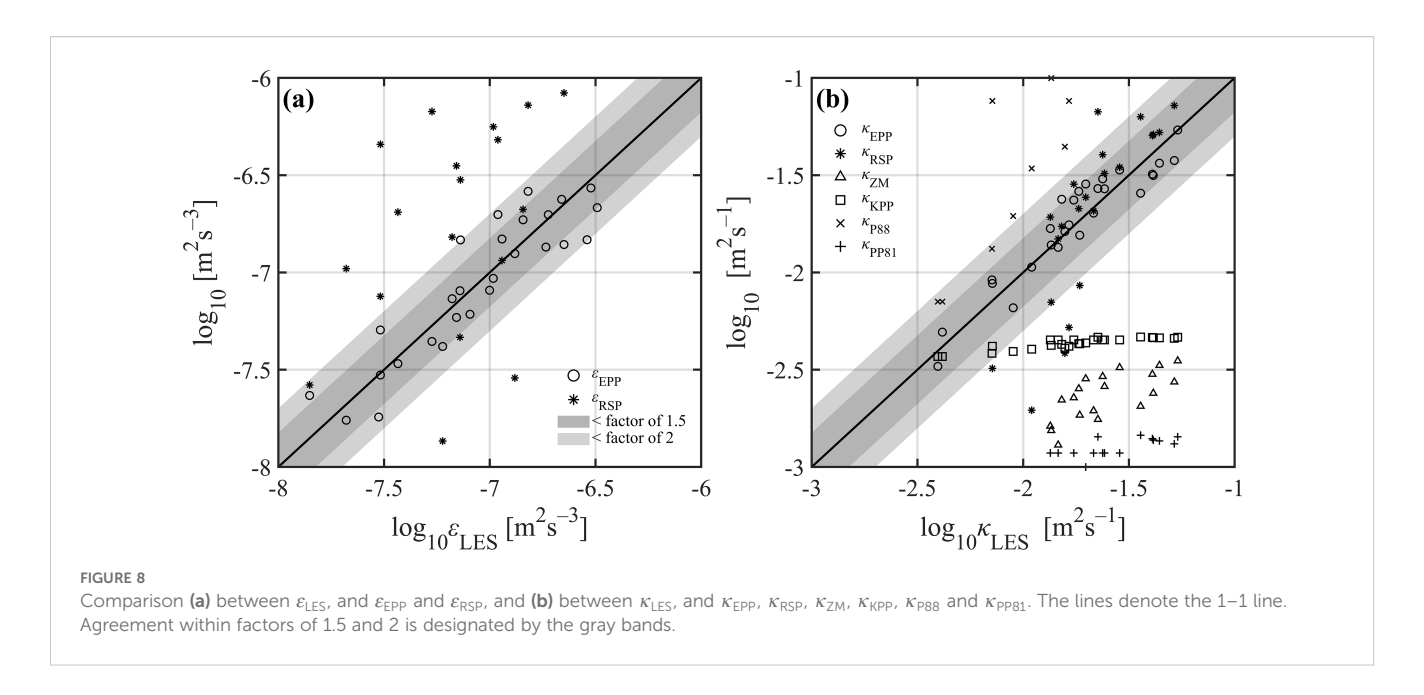
To evaluate the EPP scheme, the parameterized ε_{EPP} and the original ε_{LES} calculated from LES, are shown in Figure 8a. The parameterized values compare remarkably well to the values of LES. To be specific, ε_{EPP} explain about 81% of the variance of ε_{LES} . 96% of the samples show a discrepancy within a factor of 2 for ε_{EPP} , while about 70% of the samples show a discrepancy only within a factor of 1.5. The parameterized diffusivity κ_{EPP} and the LES-calculated diffusivity κ_{LES} are compared in Figure 8b. κ_{EPP} explains about 88% of the variance of κ_{LES} . 96% of the parameterized κ_{EPP} are within a factor of 1.5 to κ_{LES} .

Overall, the parameterized coefficients in the EPP scheme are in good agreement with the data calculated by LES, both in magnitude and variability.

4.2 Compare ε_{EPP} and κ_{EPP} with observations

The EPP scheme is also tested with independent observational data collected from the TIWE experiments (Lien et al., 1995). As described in section 2.6, 33 turbulent events similar to category 1 below the boundary layer (ML and deep cycle layer) are identified for the TIWE data (white squares in Figure 4).

When applying EPP to the IUL with $Ri \in (0, 0.25)$ that is below the boundary layer in observations, the TKE dissipation rate and diffusivity are calculated according to the schematic in Figure 3b.



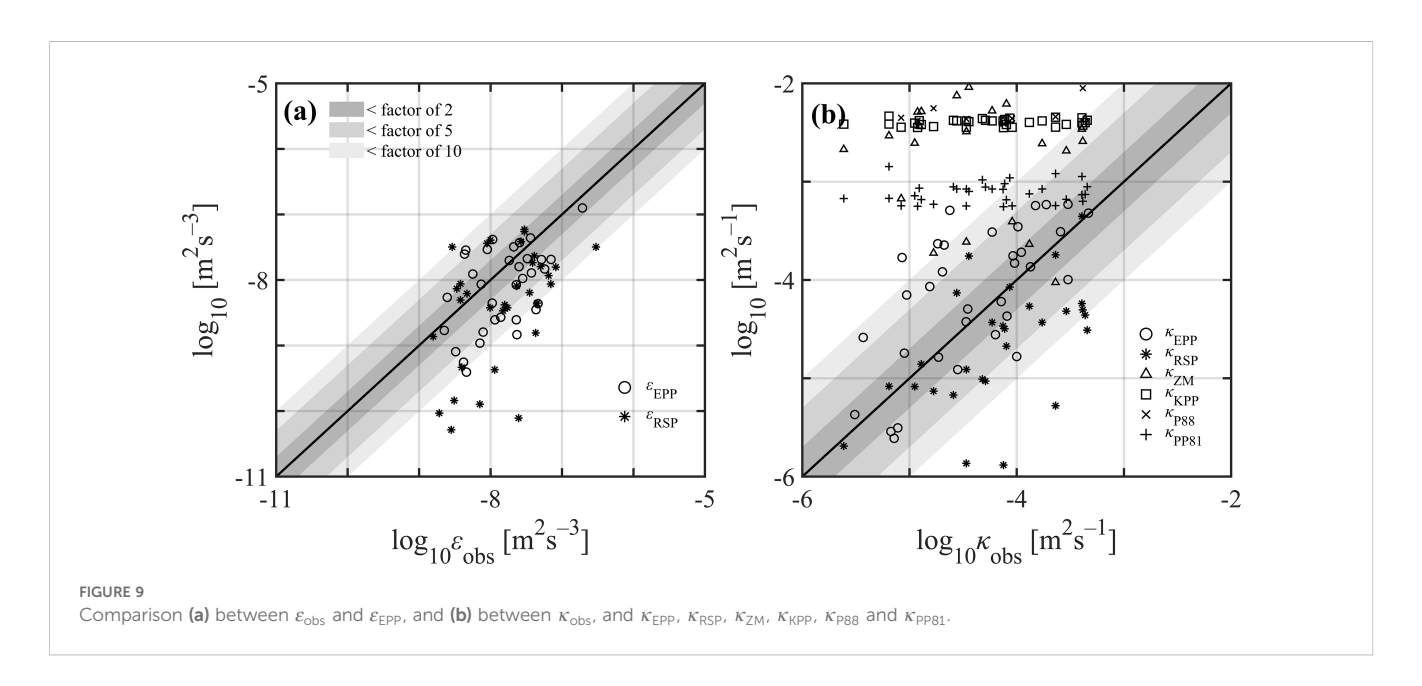
Firstly, the temperature, salinity, and velocity u_0 within the IUL can be used to calculate the initial variables, such as $\overline{N_0}$, $\overline{S_0}$ and $\overline{Ri_0}$. Next, λ_{1_P} , λ_{2_P} , λ_{3_P} , K_a , τ_P , N_P and η_P can be obtained with Equations 10, 11, 14. Using these variables and Equations 12, 13, the vertical average ε_{EPP} and κ_{EPP} are calculated. Secondly, h_0 is regarded as the sum of grid spacings of IUL. Multiplying h_0 by the ratio η_P , the TPT and grids within which the turbulence can penetrate are obtained. Finally, by multiplying κ_{EPP} by the normalized profile from Equation 15, the κ_{EPP} profile is obtained. It is worth noting that, possibly due to the influence of other forcings, the stratification within turbulent events is not always smaller than the initial value $\overline{N_0}$ as in LES. Therefore, we use the observed buoyancy frequency as N_P .

Applying the EPP to the 33 turbulent events, it is seen that the parameterized values can basically capture the magnitude and amplitude of the observed ε_{obs} and κ_{obs} (Figure 9). The agreements

between ε_{EPP} and ε_{obs} , and between κ_{EPP} and κ_{obs} are both within a factor of 10 for about 88% and a factor of 5 for about 70%, respectively. Nonetheless, the EPP shows advantages compared to the widely used previous schemes, which is discussed in the next subsection.

4.3 Compare ε_{EPP} and κ_{EPP} with previous schemes

Several previous parameterizations, including RSP, ZM (Zaron and Moum, 2009), PP81, P88 and KPP are compared, which shows an overall better performance of EPP. REV parameterization is used for ZM while shear instability mixing component of KPP is adopted for comparison. Through the comparison, we also analyze the underlying mechanisms why EPP performs better.



As shown in Figure 8a, if taking the LES as metrics, ε_{RSP} overestimates ε_{LES} , and has a larger scatter than ε_{EPP} , while only 59.3% of κ_{RSP} are within a factor of 2, compared to the 100% of ε_{EPP} . This may be due to the large inverse timescale employed in the RSP scheme, which results in a large ε_{RSP} , but its smaller γ partially offsets this overestimation. κ_{KPP} , κ_{PP81} and κ_{ZM} all underestimate the κ_{LES} by a factor of 4–18 on average, while κ_{P88} overestimates them by a factor of 18. KPP, PP81, and ZM all prescribe distinct yet nearly invariant diffusivity when the Ri< 0.25 based on observed averages. Their empirical rigidity neglecting turbulence-scale dynamics in idealized LES experiments. For P88, the overestimation stems from its mathematical formulation where κ_{P88} tends toward infinity as Ri approaches 0. The EPP seems to best fit the data, this is because this scheme fully considers the dynamical variables in addition to $\overline{Ri_0}$.

As for the parameterizations of the observations (Figure 9a), more of ε_{RSP} underestimates ε_{obs} than ε_{EPP} , but about 72% of ε_{RSP} approximate ε_{obs} well. 73% of the parameterized κ_{RSP} are within a factor of 10, while 58% of the samples are within a factor of 5. Compared with ε_{EPP} , more of κ_{RSP} underestimate κ_{obs} . κ_{ZM} , κ_{KPP} , κ_{PP81} and κ_{P88} overestimate κ_{obs} by more than a factor of 10 on average, and they fail to capture the variability of κ_{obs} . The fact that variability of turbulent diffusivity depends not only on Ri_0 but also on other variables such as shear and stratification (Richards et al., 2021) is obviously missed in these parametrizations. κ_{KPP} and κ_{PP81} overestimate κ_{obs} , indicating that KPP and PP81 must adjust their parameters according to the observations at different conditions to achieve the best parameterization, but it is almost impossible to experience all different conditions. In contrast, the EPP and RSP is relatively adaptive to the observations and LES data.

5 Summary and discussion

Shear-driven turbulence in the interior stratified shear flow is an important process in the ocean, but it is difficult to measure and simulate in ocean models. The existing parameterizations for turbulent diffusivity are usually based on the background gradient Richardson number only, which is not sufficient to capture the strength and variability of turbulence intensity.

For shear-driven turbulence in the internal ocean with $Ri \subseteq$ (0, 0.25), we present a new energy-constrained profile parameterization, EPP. The parameterization includes both the TKE dissipation rate ε and the diffusivity κ . EPP is based on an energy-constrained framework, which assumes that the TKE dissipation rate ε is proportional to both the available kinetic energy K_a and the inversed turbulent timescale τ_{LES}^{-1} . K_a is defined as the difference between the initial kinetic energy of the unstable flow and the kinetic energy of the corresponding idealized marginally stable flow. τ_{LES} is a function of both the background buoyancy frequency $\overline{N_0}$ and shear $\overline{S_0}$. The parameterization also includes 2 factors, λ_{1_p} and λ_{2_p} , both of which depend on Ri_0 , and denote the ratio of the energy transferred via shear production $E_{SP_{LES}}$ to K_a, and the ratio of the energy transferred via turbulent dissipation $E_{\mathcal{E}_{LES}}$ to $E_{SP_{LES}}$, respectively. Similarly, introducing the ratio of the energy transferred via buoyancy production $E_{B_{LES}}$ to

 $E_{\text{SP}_{\text{LES}}}$, the corresponding vertical diffusivity κ is also parameterized by the variables mentioned above (Equation 13).

Such turbulence events are observed under the surface boundary layer, such as subsurface turbulent mixing in the eastern equatorial Pacific and western boundary currents. Jia et al. (2021) suggested that a high vertical resolution model can capture many characteristics of smallscale velocity and density in the upper ocean. A lot of unstable flows of $Ri \in (0, 0.25)$ can be simulated in future numerical models with much higher vertical resolution than now. The increased shear-driven turbulent mixing is expected to be reasonably represented by this new parameterization. However, the transferability of EPP to larger-scale or more complex oceanic environments remains constrained by two key limitations: (1) The omission of rotational effects, which may distort energy cascades in mid-latitude western boundary currents; (2) Its calibration against limited-depth LES (≤ 256 m), potentially restricting its capacity to adequately capture deep-ocean processes such as mixing driven by internal wave breaking. Future iterations need incorporate rotational terms and extend validation to the full water column.

Furthermore, because the shear-driven turbulence can penetrate vertically from the layer of the low Ri to a thick surrounding layer, the thickness of which is denoted as TPT. The TPT could be several times the IULT, and may exceed several grid spacings in the numerical model. Thus, we propose a method to parameterize TPT according to initial variables, and hence construct a function of the normalized profile κ_{\star} within the TPT. Introducing TPT in the EPP scheme is certainly a step forward in improving the simulation of turbulent mixing on adjacent layers. This means that the turbulent mixing may provide an additional independent factor affecting the surrounding environment; the effect on the temperature/salinity change to the neighboring grid could be large or small, depending on whether it dominates other terms. The parameterization is calibrated using LES and tested using equatorial observations. The results show that the new parameterization can capture the variability and magnitude of turbulence, and performs better than widely-used parameterizations. Given that RSP and EPP are both based on the energy constraint framework, RSP can serve as a viable alternative to EPP. The concise formulation of RSP enables high computational efficiency. Specifically, the diffusivity derived from RSP can be combined with the diffusivity profile function of the EPP scheme. This hybrid scheme provides a practical and efficient alternative to the original EPP. The application of this parameterization in a highresolution numerical model will be reported later.

Data availability statement

The datasets presented in this study can be found in online repositories. The names of the repository/repositories and accession number(s) can be found below: https://doi.org/10.5281/zenodo. 15064783 and https://microstructure.ucsd.edu/#/cruise/32WC19911104.

Author contributions

LL: Data curation, Writing - original draft, Investigation. CL: Writing - review & editing, Conceptualization.

RH:Writing – review & editing. FW: Funding acquisition, Writing – review & editing.

Funding

The author(s) declare that financial support was received for the research and/or publication of this article. This study is supported by National Natural Science Foundation of China (42090040), National Natural Science Foundation of China (42430403), the Key Research Program of Laoshan Laboratory (LSL) (2022LSL010302), and the National Key R&D Program of China (2022YFF0801404).

Acknowledgments

The authors would like to thank two anonymous reviewers for providing insightful comments. We acknowledge the technical support from Oceanographic Data Center, IOCAS.We acknowledge the TIWE team that contributed to the collection of the TIWE microstructure data.

Conflict of interest

The authors declare that the research was conducted in the absence of any commercial or financial relationships that could be construed as a potential conflict of interest.

References

Chang, Y. S., Xu, X., Özgökmen, T. M., Chassignet, E. P., Peters, H., and Fischer, P. F. (2005). Comparison of gravity current mixing parameterizations and calibration using a high-resolution 3D nonhydrostatic spectral element model. *Ocean Model.* 10, 342–368. doi: 10.1016/j.ocemod.2004.11.002

Geyer, W. R., Lavery, A. C., Scully, M. E., and Trowbridge, J. H. (2010). Mixing by shear instability at high Reynolds number. *Geophysical Res. Lett.* 37. doi: 10.1029/2010gl045272

Hazel, P. (1972). Numerical studies of the stability of inviscid stratified shear flows. *J. Fluid Mechanics* 51, 39-61. doi: 10.1017/s0022112072001065

Howard, L. N. (1961). Note on a paper of john W. Miles. J. Fluid Mechanics 10, 509–512. doi: 10.1017/S0022112061000317

Inoue, R., Lien, R.-C., and Moum, J. N. (2012). Modulation of equatorial turbulence by a tropical instability wave. *J. Geophysical Research: Oceans* 117. doi: 10.1029/2011;007767

Inoue, R., and Smyth, W. D. (2009). Efficiency of mixing forced by unsteady shear flow. *J. Phys. Oceanography* 39, 1150–1166. doi: 10.1175/2008jpo3927.1

Jia, Y., Richards, K. J., and Annamalai, H. (2021). The impact of vertical resolution in reducing biases in sea surface temperature in a tropical Pacific Ocean model. *Ocean Model.* 157, 101722. doi: 10.1016/j.ocemod.2020.101722

Kaltenbach, H.-J., Gerz, T., and Schumann, U. (1994). Large-eddy simulation of homogeneous turbulence and diffusion in stably stratified shear flow. *J. Fluid Mechanics* 280, 1–40. doi: 10.1017/s0022112094002831

Klemp, J. B., and Durran, D. R. (1983). An upper boundary condition permitting internal gravity wave radiation in numerical mesoscale models. *Monthly Weather Rev.* 111, 430–444. doi: 10.1175/1520-0493(1983)111<0430:Aubcpi>2.0.Co;2

Kunze, E. (2014). The relation between unstable shear layer thicknesses and turbulence lengthscales. *J. Mar. Res.* 72, 95–104. doi: 10.1357/002224014813758977

Kunze, E., Williams, A. J., and Briscoe, M. G. (1990). Observations of shear and vertical stability from a neutrally buoyant float. *J. Geophysical Res.* 95, 18127. doi: 10.1029/jc095ic10p18127

Generative AI statement

The author(s) declare that no Generative AI was used in the creation of this manuscript.

Any alternative text (alt text) provided alongside figures in this article has been generated by Frontiers with the support of artificial intelligence and reasonable efforts have been made to ensure accuracy, including review by the authors wherever possible. If you identify any issues, please contact us.

Publisher's note

All claims expressed in this article are solely those of the authors and do not necessarily represent those of their affiliated organizations, or those of the publisher, the editors and the reviewers. Any product that may be evaluated in this article, or claim that may be made by its manufacturer, is not guaranteed or endorsed by the publisher.

Supplementary material

The Supplementary Material for this article can be found online at: https://www.frontiersin.org/articles/10.3389/fmars.2025.1615741/full#supplementary-material

Large, W. G., Mcwilliams, J. C., and Doney, S. C. (1994). Oceanic vertical mixing: A review and a model with a nonlocal boundary layer parameterization. *Rev. Geophysics* 32, 363. doi: 10.1029/94rg01872

Lien, R.-C., Caldwell, D. R., Gregg, M. C., and Moum, J. N. (1995). Turbulence variability at the equator in the central Pacific at the beginning of the 1991–1993 El Niño. *J. Geophysical Res.* 100, 6881. doi: 10.1029/94jc03312

Miles, J. W. (1961). On the stability of heterogeneous shear flows. J. Fluid Mechanics 10, 496–508. doi: 10.1017/S0022112061000305

Moeng, C.-H. (1984). A large-eddy-simulation model for the study of planetary boundary-layer turbulence. *J. Atmospheric Sci.* 41, 2052–2062. doi: 10.1175/1520-0469 (1984)041<2052:Alesmf>2.0.Co;2

Moum, J. N. (1996a). Efficiency of mixing in the main thermocline. J. Geophysical Research: Oceans 101, 12057–12069. doi: 10.1029/96jc00508

Moum, J. N. (1996b). Energy-containing scales of turbulence in the ocean thermocline. *J. Geophysical Research: Oceans* 101, 14095–14109. doi: 10.1029/96ic00507

Moum, J. N., Gregg, M. C., Lien, R. C., and Carr, M. E. (1995). Comparison of turbulence kinetic energy dissipation rate estimates from two ocean microstructure profilers. *J. Atmospheric Oceanic Technol.* 12, 346–366. doi: 10.1175/1520-0426(1995) 012-0346:COTKED>2.0.CO;2

Moum, J. N., Hebert, D., Paulson, C. A., and Caldwell, D. R. (1992). Turbulence and internal waves at the equator. Part I: statistics from towed thermistors and a microstructure profiler. *J. Phys. Oceanography* 22, 1330–1345. doi: 10.1175/1520-0485(1992)022<1330:taiwat>2.0.co;2

Osborn, T. R. (1980). Estimates of the local rate of vertical diffusion from dissipation measurements. *J. Phys. Oceanography* 10, 83–89. doi: 10.1175/1520-0485(1980) 010<0083:Eotlro>2.0.Co;2

Pacanowski, R. C., and Philander, S. G. H. (1981). Parameterization of vertical mixing in numerical models of tropical oceans. *J. Phys. Oceanography* 11, 1443–1451. doi: 10.1175/1520-0485(1981)011<1443:Povmin>2.0.Co;2

Penney, J., Morel, Y., Haynes, P., Auclair, F., and Nguyen, C. (2020). Diapycnal mixing of passive tracers by Kelvin–Helmholtz instabilities. *J. Fluid Mechanics* 900. doi: 10.1017/jfm.2020.483

Peters, H., Gregg, M. C., and Toole, J. M. (1988). On the parameterization of equatorial turbulence. *J. Geophysical Res.* 93, 1199. doi: 10.1029/jc093ic02p01199

Pham, H. T., and Sarkar, S. (2022). A comparative study of turbulent stratified shear layers: effect of density gradient distribution. *Environ. Fluid Mechanics*. doi: 10.1007/s10652-022-09873-2

Pham, H. T., Sarkar, S., Smyth, W. D., Moum, J. N., and Warner, S. J. (2024). Deep-cycle turbulence in the upper pacific equatorial ocean: characterization by LES and heat flux parameterization. *J. Phys. Oceanography* 54, 577–599. doi: 10.1175/JPO-D-23-0015.1

Polzin, K. (1996). Statistics of the richardson number: mixing models and finestructure. *J. Phys. Oceanography* 26, 1409–1425. doi: 10.1175/1520-0485(1996) 026<1409:SOTRNM>2.0.CO;2

Richards, K. J., Natarov, A., and Carter, G. S. (2021). Scaling of shear-generated turbulence: the equatorial thermocline, a case study. *J. Geophysical Research: Oceans* 126. doi: 10.1029/2020jc016978

Salehipour, H., and Peltier, R. (2015). Diapycnal diffusivity, turbulent Prandtl number and mixing efficiency in Boussinesq stratified turbulence. *J. Fluid Mechanics* 775, 464–500. doi: 10.1017/jfm.2015.305

Shih, L. H., Koseff, J. R., Ivey, G. N., and Ferziger, J. H. (2005). Parameterization of turbulent fluxes and scales using homogeneous sheared stably stratified turbulence simulations. *J. Fluid Mechanics* 525, 193–214. doi: 10.1017/s0022112004002587

Smyth, W. D. (2020). Marginal instability and the efficiency of ocean mixing. *J. Phys. Oceanography* 50, 2141–2150. doi: 10.1175/jpo-d-20-0083.1

Smyth, W. D., Carpenter, J. R., and Lawrence, G. A. (2007). Mixing in symmetric holmboe waves. *J. Phys. Oceanography* 37, 1566–1583. doi: 10.1175/jpo3037.1

Smyth, W. D., and Moum, J. N. (2012). Ocean mixing by kelvin-helmholtz instability. *Oceanography* 25, 140–149. doi: 10.5670/oceanog.2012.49

Smyth, W. D., Moum, J. N., and Caldwell, D. R. (2001). The efficiency of mixing in turbulent patches: inferences from direct simulations and microstructure observations. *J. Phys. Oceanography* 31, 1969–1992. doi: 10.1175/1520-0485(2001)031<1969:teomit>2.0.co;2

Smyth, W. D., Nash, J. D., and Moum, J. N. (2005). Differential diffusion in breaking kelvin–helmholtz billows. *J. Phys. Oceanography* 35, 1004–1022. doi: 10.1175/jpo2739.1

Smyth, W. D., and Peltier, W. R. (1989). The transition between kelvin-helmholtz and holmboe instability: an investigation of the overreflection hypothesis. J.

Atmospheric Sci. 46, 3698-3720. doi: 10.1175/1520-0469(1989)046<3698: ttbkah>2.0.co:2

Smyth, W. D., and Winters, K. B. (2003). Turbulence and mixing in holmboe waves. J. Phys. Oceanography 33, 694–711. doi: 10.1175/1520-0485(2003)33<694:

Sullivan, P., Mcwilliams, J., and Moeng, C. (1996). A grid nesting method for large-eddy simulation of planetary boundary layer flows. *Boundary Layer Meteorology* 80, 167–202. doi: 10.1007/BF00119016

Thorpe, S. A. (1973). Experiments on instability and turbulence in a stratified shear flow. *J. Fluid Mechanics* 61, 731–751. doi: 10.1017/s0022112073000911

Thorpe, S. A., and Liu, Z. (2009). Marginal instability? J. Phys. Oceanography 39, 2373–2381. doi: 10.1175/2009jpo4153.1

Tong, B., Guo, J., Wang, Y., Li, J., Yun, Y., Solanki, R., et al. (2022). The near-surface turbulent kinetic energy characteristics under the different convection regimes at four towers with contrasting underlying surfaces. *Atmospheric Res.* 270, 106073. doi: 10.1016/j.atmosres.2022.106073

Tu, J., Wu, J., Fan, D., Liu, Z., Zhang, Q., and Smyth, W. (2024). Shear instability and turbulent mixing by kuroshio intrusion into the changjiang river plume. *Geophysical Res. Lett.* 51. doi: 10.1029/2024gl110957

Wang, D., Large, W. G., and McWilliams, J. C. (1996). Large-eddy simulation of the equatorial ocean boundary layer: Diurnal cycling, eddy viscosity, and horizontal rotation. *J. Geophysical Research: Oceans* 101, 3649–3662. doi: 10.1029/95jc03441

Wang, D., McWilliams, J. C., and Large, W. G. (1998). Large-eddy simulation of the diurnal cycle of deep equatorial turbulence. *J. Phys. Oceanography* 28, 129–148. doi: 10.1175/1520-0485(1998)028<0129:Lesotd>2.0.Co;2

Wang, D., and Müller, P. (2002). Effects of equatorial undercurrent shear on upper-ocean mixing and internal waves. *J. Phys. Oceanography* 32, 1041–1057. doi: 10.1175/1520-0485(2002)032<1041:Eoeuso>2.0.Co;2

Watanabe, T., and Nagata, K. (2021). Large-scale characteristics of a stably stratified turbulent shear layer. *J. Fluid Mechanics* 927. doi: 10.1017/jfm.2021.773

Winters, K. B., Lombard, P. N., Riley, J. J., and D'Asaro, E. A. (1995). Available potential energy and mixing in density-stratified fluids. *J. Fluid Mechanics* 289, 115–128. doi: 10.1017/s002211209500125x

Zaron, E. D., and Moum, J. N. (2009). A new look at richardson number mixing schemes for equatorial ocean modeling. *J. Phys. Oceanography* 39, 2652–2664. doi: 10.1175/2009jpo4133.1